

Brownian Dynamics Simulation Study on the Anisotropic FENE Dumbbell Model for Concentrated Polymer Solution and the Melt

Hoon Goo Sim, Chang Jun Lee, Woon Chun Kim, and Hyungsuk Pak*

Department of Chemistry, Seoul National University, Seoul 151-742, Korea

Received March 27, 2000

We study the rheological properties of concentrated polymer solution and the melt under simple shear and elongational flow using Brownian dynamics simulation. In order to describe the anisotropic molecular motion, we modified the Giesekus' mobility tensor by incorporating the finitely extensible non-linear elastic (FENE) spring force into dumbbell model. To elucidate the nature of this model, our simulation results are compared with the data of FENE-P ("P" stands for the Perterin) dumbbell model and experiments. While in steady state both original FENE and FENE-P models exhibit a similar viscosity response, the growth of viscosity becomes dissimilar as the anisotropy decreases and the flow rate increases. The steady state viscosity obtained from the simulation well describes the experiments including the shear-thinning behavior in shear flow and viscosity-thinning behavior in elongational flow. But the growth of viscosity of original FENE dumbbell model cannot describe the experimental results in both flow fields.

Introduction

The molecular motions in concentrated polymer solution and the melt are complex because of the intermolecular interactions between different chains. In recent years, de Gennes,¹ Doi,^{2,3} and Curtiss *et al.*⁴ have described the chain motion in such a topologically interacting system. In order to derive the theoretical formula, they assumed that the molecular motion in the direction of the chain contour might be easier than the motion perpendicular to it. Giesekus⁵ also used the assumption of anisotropic molecular motion in order to derive the constitutive equation for polymeric liquids. One-mode simple Giesekus' model well predicted the steady state viscosity and the growth of shear viscosity.^{5-b,c} However, in elongational flow field, his simple model could not show the characteristic behaviors of polymeric liquids such as strain-hardening in transient state and viscosity-thinning in steady state. To overcome the oversimplified one-mode simple model, he introduced the relaxation-type dependence of the mobility^{5-d} on the configuration tensor.

The same constitutive equation of simple Giesekus' model can be also derived in terms of the phase-space kinetic theory⁶ of polymeric liquids if we consider a polymer chain as a Hookian dumbbell which consists of two identical beads connected by a massless spring named connector vector. The linear Hookean spring force is realistic only for small deformation from the equilibrium. Whereas the dumbbell with Hookean spring is infinitely extensible, real polymers can certainly be extended to their fully stretched length at most. For large extension of a polymer the linear spring-force law is a poor approximation, so it can be improved by introducing the FENE spring force.⁷ Dumbbell models with FENE spring force are now widely used in numerical flow calculations; both in the classical approach *via* a closed constitutive equation⁸ and in a new approach in which the polymeric stress tensors are computed *via* Brownian dynamics (BD)

simulation.⁹

Wiest¹⁰ modified the Giesekus constitutive equation by incorporating the finite extensibility of polymer chains into the dumbbell kinetic theory. The modified constitutive equation quantitatively described the steady state viscosity in the shear and elongational flow, but could not reproduce the growth of viscosity in elongational flow. When he modified the constitutive equation, he used the FENE-P¹¹ spring force in order to obtain an analytically more tractable constitutive equation because no closed constitutive equation for the polymeric stress tensor exists and no simple analytical solutions are possible for original FENE dumbbell model.

In this paper, we use the Brownian dynamics simulation method to obtain the polymeric stress tensors for the original FENE dumbbell model with the anisotropic mobility tensor. We also derive the constitutive equation in simple form for the FENE-P dumbbell model using the phase-space kinetics theory. From the Brownian dynamics simulation, we obtain the growth of and steady state viscosity for simple shear and elongational flow. These results will be compared with those of FENE-P dumbbell model and experimental data.

Constitutive equation for the FENE-P dumbbell model

The diffusion equation of configurational distribution function $\psi(\mathbf{Q}, t)$ ^{4-d} for connector vectors $\mathbf{Q} = \mathbf{r}_2 - \mathbf{r}_1$ of anisotropic dumbbells can be represented by:

$$\frac{\partial \psi}{\partial t} = - \frac{\partial}{\partial \mathbf{Q}} \cdot \left\{ \boldsymbol{\kappa} \cdot \mathbf{Q} \psi - 2k_B T \boldsymbol{\zeta}^{-1} \cdot \left[\frac{\partial}{\partial \mathbf{Q}} \cdot \boldsymbol{\xi}^{-1} \psi \right] - 2 \boldsymbol{\zeta}^{-1} \cdot \mathbf{F}^{(c)} \psi \right\} \quad (1)$$

where $\boldsymbol{\kappa}$ is the transpose of macroscopic velocity gradient, k_B is the Boltzmann constant, T is the absolute temperature, $\boldsymbol{\zeta}^{-1}$ is the anisotropic mobility tensor, $\boldsymbol{\xi}^{-1}$ is a tensor for the

anisotropic Brownian motion, and $\mathbf{F}^{(c)}$ is the connector force. In order to represent the anisotropic molecular motion, we use the anisotropic mobility tensor, $\boldsymbol{\zeta}^{-1}$, suggested by Giesekus^{5-b} in terms of the macroscopic quantity:

$$\boldsymbol{\zeta}^{-1} = \frac{1}{\zeta} \left(\boldsymbol{\delta} - \frac{\alpha}{nk_B T} \boldsymbol{\tau}_p \right) \quad (2)$$

where ζ is the friction coefficient of a bead, $\boldsymbol{\delta}$ is a unit tensor, α is an anisotropy parameter, n is the number density of polymer molecules, and $\boldsymbol{\tau}_p$ is the stress tensor contributed from polymer molecules. If we assume the Brownian motion is isotropic ($\boldsymbol{\zeta}^{-1} = \boldsymbol{\delta}$), we can obtain the polymer contribution to the stress tensor of Kramers expression:^{4-d}

$$\boldsymbol{\tau}_p = nk_B T \boldsymbol{\delta} - n \langle \mathbf{Q} \mathbf{F}^{(c)} \rangle \quad (3)$$

where the angular brackets indicate an ensemble average over all \mathbf{Q} using $\psi(\mathbf{Q}, t)$.

Warner⁷ proposed the following original FENE spring force:

$$\mathbf{F}^{(c)} = \frac{H\mathbf{Q}}{1 - (Q/Q_0)^2}, \quad (Q \leq Q_0) \quad (4)$$

where H is the spring constant, Q is the length of connector vector, and Q_0 is the maximum extensible spring length. When this original spring force is applied to Eq. (1), no closed constitutive equation for the polymeric stress tensor exists and no simple analytical solution is possible. Therefore, we will evaluate the average of the stress tensor via Brownian dynamics simulation.¹²⁻¹³ An analytically more tractable dumbbell model which leads to a closed constitutive equation can be obtained by replacing the configuration-dependent non-linear factor in the FENE spring force with a self-consistently averaged term. The FENE-P ("P" stands for Peterlin¹¹ who introduced this idea) approximation for FENE spring force is expressed as:

$$\mathbf{F}^{(c)} = \frac{H\mathbf{Q}}{1 - \langle (Q/Q_0)^2 \rangle}, \quad (Q \leq Q_0) \quad (5)$$

Using the FENE-P spring force, we obtain the closed constitutive equation

$$\boldsymbol{\tau}_p^* + (Z \boldsymbol{\tau}_p^*)_{(1)} - \alpha \{ \boldsymbol{\tau}_p^* \cdot \boldsymbol{\tau}_p^* \} = (Z \boldsymbol{\delta})_{(1)}, \quad Z = \frac{b}{b + 3 - Tr(\boldsymbol{\tau}_p^*)} \quad (6)$$

where $Tr(\boldsymbol{\tau}_p^*)$ is the trace of the stress tensor in reduced units, and the subscription (1) of $\Lambda_{(1)}$ denotes upper convective derivative of Λ ; $\Lambda_{(1)} = \frac{D\Lambda}{Dt} - (\boldsymbol{\kappa} \cdot \Lambda + \Lambda \cdot \boldsymbol{\kappa}^T)$, here D/Dt is the material time derivative and $\boldsymbol{\kappa}^T$ is the transpose of $\boldsymbol{\kappa}$. This constitutive equation is equivalent to Eq. (8) of Wiest¹⁰ if we express the parameter Z into reciprocal form. In deriving Eq. (6), we used the reduced units: time $t = \lambda_{Hf}^*$,

$\lambda_H = \zeta/4H$, length $\mathbf{Q} = l\mathbf{Q}^*$, $l^2 = k_B T/H$, finite extensibility parameter $b = HQ_0^2/k_B T$, and stress tensor $\boldsymbol{\tau}_p = nk_B T \boldsymbol{\tau}_p^*$. Hereafter, we will express the physical quantities in reduced units without any superscripts.

Brownian dynamics simulation for original FENE dumbbell

When we assume the Brownian motion is isotropic ($\boldsymbol{\zeta}^{-1} = \boldsymbol{\delta}$), Eq. (1) is equivalent to the Ito stochastic differential equation¹⁴ (SDE) for a three-dimensional Markov process \mathbf{Q} :

$$d\mathbf{Q} = \left(\boldsymbol{\kappa} \cdot \mathbf{Q} - \frac{1}{2} \boldsymbol{\zeta}^{-1} \cdot \frac{\mathbf{Q}}{1 - (Q^2/b)} \right) dt + \mathbf{B} \cdot d\mathbf{W} \quad (7)$$

where $\boldsymbol{\zeta}^{-1} = \boldsymbol{\delta} - \alpha \boldsymbol{\tau}_p$, $\mathbf{B} \cdot \mathbf{B}^T = \boldsymbol{\zeta}^{-1}$, $\langle \mathbf{W}(t) \rangle = \mathbf{0}$, and $\langle \mathbf{W}(t_1) \mathbf{W}(t_2) \rangle = \min(t_1, t_2) \boldsymbol{\delta}$.

The Wiener process \mathbf{W} is the 3-dimensional Gaussian process of which first moment is zero vector and second moment is a diagonal matrix whose element is minimum time between two Wiener processes. The first term of right side of Eq. (7) is that of the deterministic ordinary differential equation (ODE), and referred as drift term. The Brownian motion of dumbbell causes Wiener process that distinguishes the SDE from the ODE, so the second term is referred as diffusion term. Since the non-linear Eq. (7) cannot be solved analytically, we have to integrate it numerically. The simplest numerical method to integrate Eq. (7) is the Euler scheme.¹⁴ For a given timestep Δt , the Euler scheme is given by

$$\mathbf{Q}(t + \Delta t) = \mathbf{Q}(t) + \left(\boldsymbol{\kappa}(t) \cdot \mathbf{Q}(t) - \frac{1}{2} \boldsymbol{\zeta}^{-1} \cdot \frac{\mathbf{Q}(t)}{1 - (Q(t)^2/b)} \right) \Delta t + \mathbf{B}(t) \cdot \Delta \mathbf{W} \quad (8)$$

where the increment $\Delta \mathbf{W} = \mathbf{W}(t + \Delta t) - \mathbf{W}(t)$ is an independent 3-dimensional Gaussian process that has the same statistical properties in Eq. (7).

During the simulation according to Eq. (8), there is a certain probability that the connector vector exceeds the allowed spring extension for FENE dumbbell model. To avoid such unphysical range, we use the predictor-corrector Euler method.¹⁴ At low flow rate, the diffusion term introduces the fluctuation into the ensemble averaged stress tensor, which appears as unwanted "noise". This noise severely limits our ability to calculate low flow rate viscosity, where the signal to noise ratio becomes very small. This undesirable noise can be reduced by variance reduction method¹⁵; we run a parallel equilibrium simulation (*i.e.* $\boldsymbol{\kappa} = \mathbf{0}$) from the same initial configurations and with the same stochastic displacements (*i.e.* $\mathbf{W}^{eq} = \mathbf{W}$), then we obtain the variance reduced stress tensor by subtracting equilibrium values from the stress tensor calculated from the non-equilibrium simulation.

Before closing this section we briefly define the flow situ-

ations and the material functions that we investigate. In simple shear flow, the velocity field is given by $v_x = \dot{\gamma}y$, $v_y = 0$, and $v_z = 0$, where $\dot{\gamma}$ is the shear rate and may be time dependent. At inception of shear flow, the system is initially at equilibrium and the stress tensor vanishes. For time $t \geq 0$, a constant shear rate $\dot{\gamma}_0$ is applied and the stresses grow until they reach their steady state values. In this case, we define three time-dependent material functions such as viscosity η^+ , first normal stress coefficient Ψ_1^+ , and second normal stress coefficient Ψ_2^+ in dimensionless form: $\eta^+ = -\tau_{xy}/\dot{\gamma}_0$, $\Psi_1^+ = -(\tau_{xx} - \tau_{yy})/\dot{\gamma}_0^2$, $\Psi_2^+ = -(\tau_{yy} - \tau_{zz})/\dot{\gamma}_0^2$. In simple elongational flow, the velocity profile is given by $v_x = -\frac{1}{2}\dot{\epsilon}x$, $v_y = -\frac{1}{2}\dot{\epsilon}y$, and $v_z = +\dot{\epsilon}z$, where the elongation rate may be a function of time. For time $t \geq 0$, a time-dependent material function describing the growth of the stresses in constant positive rate $\dot{\epsilon}_0$ is defined as: $\eta^+ = -(\tau_{zz} - \tau_{xx})/\dot{\epsilon}_0$.

Results and Discussion

In this section, we compare the viscosities obtained from simulation for the original FENE model with those of FENE-P model and experimental data in both simple shear and elongational flow. In order to obtain the polymeric stress tensors of original FENE dumbbell model, we simulate 30000 dumbbells in each strain rate until the stress tensors reach their steady state values. When the strain rate is low ($\dot{\gamma}_0 < 1.0$, $\dot{\epsilon}_0 < 1.0$), we used the timestep $\Delta t = 0.01, 0.0025$ for shear and elongational flow, respectively. As the strain rate increases, the timestep decreases in inverse ratio to the strain rate: $\Delta t = 0.01/\dot{\gamma}_0, 0.0025/\dot{\epsilon}_0$. Time-dependent stress tensor contributed from polymer molecule is calculated as follows:

$$\tau_p(t) = \delta - \frac{1}{N} \sum_{i=1}^N \frac{Q_i(t)Q_i(t)}{1 - Q^2(t)/b} \quad (9)$$

where N is the number of dumbbells.

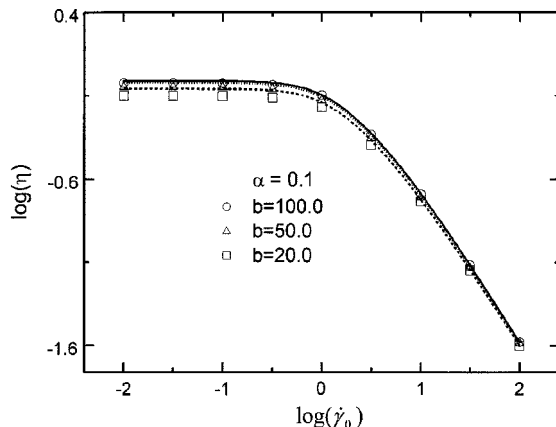


Figure 1. Shear-rate-dependent viscosity as a function of the shear rate for various finite extensibility parameters b . (Open symbols represent simulation data and line curves represent the prediction from constitutive equation)

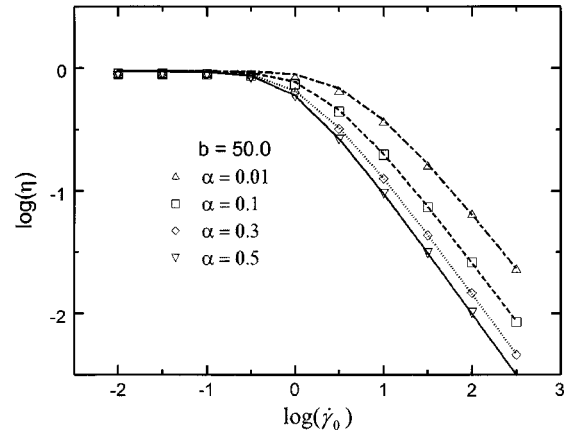


Figure 2. Shear-rate-dependent viscosity as a function of the shear rate for various anisotropy parameters α . (Open symbols represent simulation data and line curves represent the prediction from constitutive equation)

Shear flow field. Shear-rate-dependent viscosity is presented for various finite extensibility and anisotropy parameters for FENE-P and original FENE dumbbell model in Figure 1 and 2. We can see that both models exhibit very similar steady responses. The shear-rate-dependent viscosity approaches a constant value, zero-shear-rate viscosity η_0 , at low shear rates and decreases at high shear rates according to a power-law. The finite extensibility parameter has a little influence on the shear-rate-dependent viscosity. The shear-rate-dependent viscosity for both models also shows very similar responses at higher shear rate regardless of the anisotropy parameters. As the shear rate increases, the slope of power-law region has the same value of -1 as mentioned by Wiest.¹⁰ In experimental,^{4,d} however, the slope ranges between -0.4 and -0.9 in typical polymeric liquids.

In Figure 3 and 4, we present the growth of viscosity after inception of shear flow for various shear rates and anisotropy parameters. The viscosity of both models exhibits an overshoot at high shear rate before it reaches plateau region regardless of the anisotropy parameter. However, in contradiction to experimental observations,^{4,d} the lower shear rate curve cannot envelope the higher shear rate curves in both models as shown in Figure 3. The protrusions of higher rate curve over the lower rate curve become greater as the shear rate increases for both models. However, we can see that the protrusions of viscosity curve in higher shear rate gradually disappear as the anisotropy parameter increase. Figure 4 explains these behaviors. Figure 4 also shows that the maximum and plateau value of viscosity decrease as the anisotropy parameter increases. Moreover, the overshoot occurs in earlier time as the anisotropy parameter increases. The mobility tensor used in Eq. (7) can account for these behaviors. That is, as the anisotropy parameter increases under the same strain rate, the inward movement of beads caused by the spring force through the mobility tensor becomes larger; in other words, the connector vector is likely to be less deformed against the imposed strain.

The above results imply that shear-rate-dependent viscos-

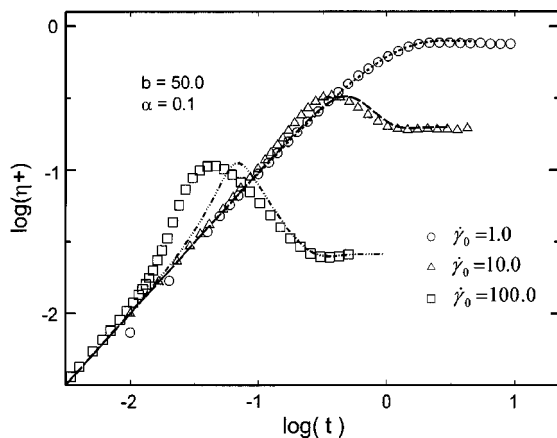


Figure 3. The growth of the viscosity after inception of shear flow for various shear rates $\dot{\gamma}_0$. (Open symbols represent simulation data and line curves represent the prediction from constitutive equation)

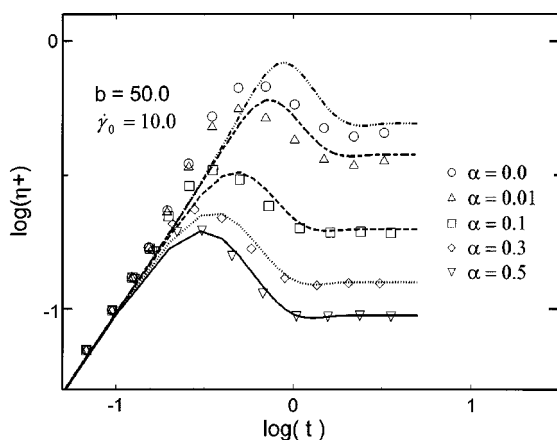


Figure 4. The growth of the viscosity after inception of shear flow for various anisotropy parameters α . (Open symbols represent simulation data and line curves represent the prediction from constitutive equation)

ity is more sensitive to the anisotropy parameter than to the extensibility parameter for both models. While both models show a similar response in steady state viscosity, the growth of viscosity of both models does not coincide with each other in overshoot region at high strain rate. Especially in small anisotropy parameter, the growth of viscosities of both models cannot predict the experimental results.

Elongational flow field. When the elongational rate is high, the distribution function of dumbbell becomes sharply peaked, thus the original FENE spring force can be approximated to the FENE-P spring force as pointed out by Tanner.¹⁶ Consequently, the steady state elongational viscosity of FENE-P model at high elongational rate will coincide with that of original FENE model.

Figure 5 and 6 show the steady state elongational viscosity for various finite extensibility and anisotropy parameters, respectively. Two models show very similar steady state responses; the elongational viscosity approaches a constant value at low elongational rate, which is three times the corre-

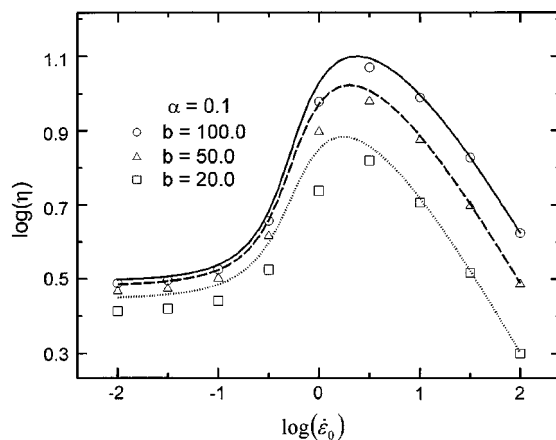


Figure 5. Steady state elongational viscosity as a function of the elongation rate for various extensibility parameters b . (Open symbols represent simulation data and line curves represent the prediction from constitutive equation)

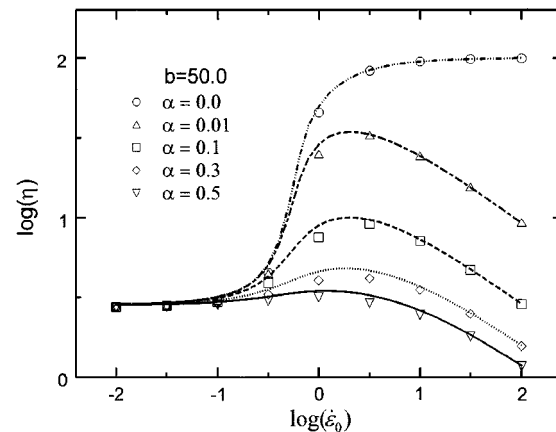


Figure 6. The steady state elongational viscosity as a function of the elongation rate for various anisotropy parameters α . (Open symbols represent simulation data and line curves represent the prediction from constitutive equation)

sponding zero-shear-rate viscosity. Contrary to the original Giesekus simple model,^{5-b} we can just find the viscosity-thinning behaviors except $\alpha = 0.0$. In Figure 5, we can see that the maximum value of viscosity increases and the curves become broad with increasing the finite extensibility parameter. Figure 6 clearly shows that the viscosity-thinning behavior occur even in a small anisotropy parameter.

The growth of the viscosity after inception of elongational flow for various elongational rates and anisotropy parameters is shown in Figure 7 and 8. As does in shear flow, the differences of viscosity for both models increase at intermediate time region regardless of the elongational rate and the anisotropy parameters. Figure 7 shows that the growth of the viscosity becomes steeper and occurs earlier in time as the elongational rate increases in both models. The viscosity of the original FENE model approaches the steady state value more smoothly than that of the FENE-P model at high elongational rate. In Figure 8, we can see that the elongational viscosity decreases as the anisotropy parameter increases.

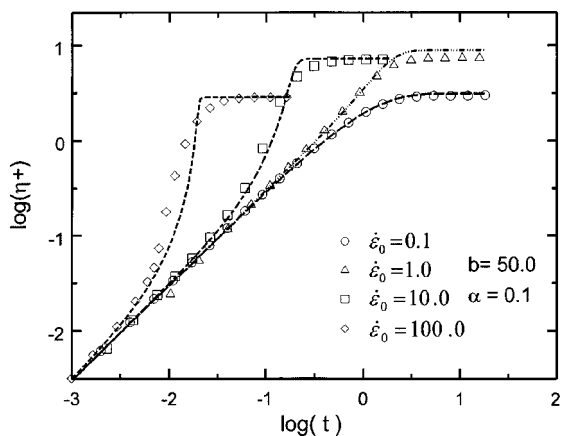


Figure 7. The growth of the viscosity after inception of elongational flow for various elongational rates $\dot{\epsilon}_0$. (Open symbols represent simulation data and line curves represent the prediction from constitutive equation)

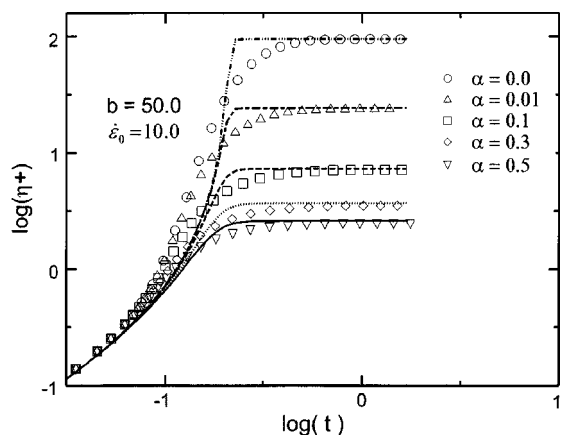


Figure 8. The growth of the viscosity after inception of elongational flow for various anisotropy parameters α . (Open symbols represent simulation data and line curves represent the prediction from constitutive equation)

However, we cannot reproduce the strain-hardening behavior at high rate regardless of any extensibility and anisotropy parameters in both models.

From the above results of shear and elongation flow, we saw that there exists discrepancy in growth of viscosity between both models, whereas the steady state viscosity is coincided with each other. These disagreements are caused by the difference of FENE spring force and the expression of stress tensor. That is to say, the non-linear force factor of the original FENE spring force increase steeply as the extension of the dumbbell is close to the allowable length. Thus some population of highly stretched dumbbells leads to the high valued stress tensor and mobility tensor. Furthermore the original FENE dumbbells response to the individual spring force, while the FENE-P dumbbells is enforced by the non-linear spring force in which the non-linear spring force factor is replaced by an averaged value. These differences of non-linear spring force and its insertion into the stress and the mobility tensor are drastically shown in Figure 7.

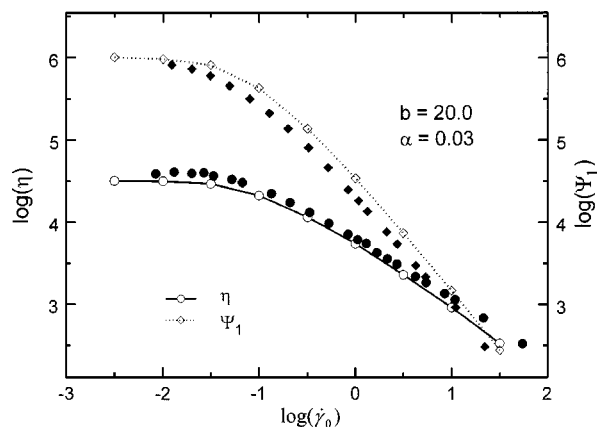


Figure 9. Comparison of the original FENE dumbbell model for the shear-rate-dependent viscosity with the data of Menezes¹⁷ for polystyrene solution. The data of dumbbells are drawn for $\lambda_H = 31.6s$ and $nkT\lambda_H = 63,095 \text{ Pa s}$. (Filled symbols represent the data of Menezes¹⁷ and line-open symbols represent the simulation data)

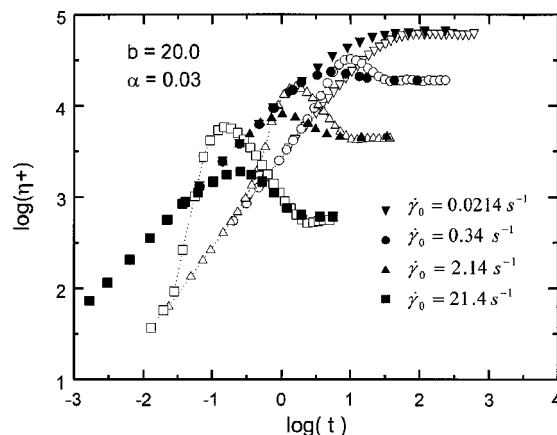


Figure 10. Comparison of the original FENE dumbbell model for the growth of shear viscosity with the data of polystyrene solution.¹⁷ The data of FENE dumbbells are drawn for $\lambda_H = 31.6s$ and $nkT\lambda_H = 79,432 \text{ Pa s}$, which are obtained when we fit the viscosity data with the experimental data in Figure 9. (Filled symbols represent the data of Menezes¹⁷ and line-open symbols represent simulation data)

Comparisons with experimental data. Besides the dependence of the viscoelasticity on the external parameters such as strain rate, time, temperature, and concentration, the rheological properties of polymeric liquid are affected by the molecular parameters: molecular weight, molecular weight distribution, and chain branching. In this section, we compare our simulation data of original FENE dumbbell model with nearly monodisperse polystyrene solution¹⁷ and melt,¹⁸ and largely polydisperse and branched low-density polyethylene melt.¹⁹

Figure 9 shows the steady state shear viscosity and first normal stress coefficient as a function of shear rate for simulation and the nearly monodisperse polystyrene solution.¹⁷ Though our simulation data describe the experimental results qualitatively, we cannot fit the data of viscosity and first

normal stress coefficient simultaneously; if we make viscosity coincided, there is a bit of discrepancies in first normal stress coefficient between simulation and experiment, and vice versa. In Figure 10, we show the start-up viscosity for the same material with the parameters with which the viscosity data are coincided in Figure 9. As we mentioned in Figure 3, that is, the viscosity curve of lower shear rate cannot envelope the high shear rate curves, the simulation data can hardly describe the experimental results except for the plateau region.

Figure 11 shows the data of Laun¹⁹ for the steady state elongational viscosity of low-density polyethylene melt, named by IUPAC-A, and the corresponding results of simulation. The agreement between the simulation results and experimental data is remarkable. With the parameters used in Figure 11, we show the growth of elongational viscosity for the same material in Figure 12. Though the steady state

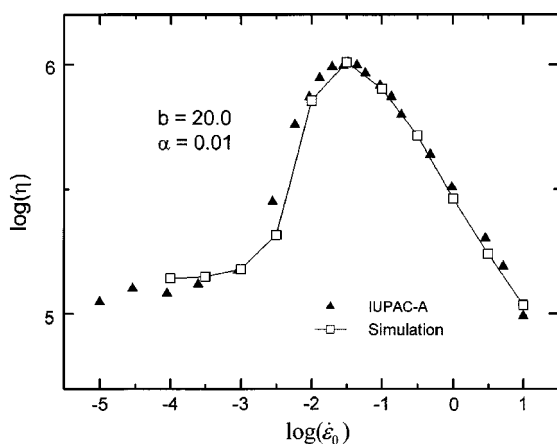


Figure 11. Comparison of the original FENE dumbbell model for the steady state elongational viscosity with the data of Laun¹⁹ for the IUPAC-A polymer melt. The data of dumbbell are drawn for $\lambda_H = 100.0$ s and $nkT\lambda_H = 56,234$ Pa s. (Filled symbols represent the data of Laun¹⁹ and line-open symbols represents the simulation data)

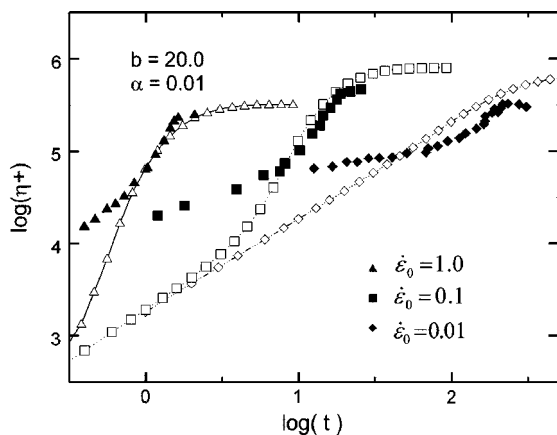


Figure 12. Comparison of the original FENE dumbbell model for the growth of viscosity with the data of Laun¹⁹ for the IUPAC-A polymer melt. The data of dumbbells are drawn for the same parameters in Figure 11. (Filled symbols represent the data of Laun¹⁹ and line-open symbols represent the simulation data)

viscosity of FENE dumbbell model coincides well with the experimental results, the behaviors of growth of viscosity cannot describe the growth of the elongational viscosity, especially in the early time region.

Figure 13 shows the data of Münstedt¹⁸ for the steady state elongational viscosity of polystyrene melt and the results of simulation. As does in IUPAC-A melts, the agreement between the results of simulation and experiment is remarkable. Using the same parameters used in Figure 13, we show the growth of viscosity for the same material in Figure 14. Though the growth of viscosity of dumbbell model cannot exactly describe the growth of the elongational viscosity for nearly monodisperse polystyrene melt, the discrepancy in the viscosity of polystyrene melt is smaller than IUPAC-A polymer melt. This is probably a consequence of the molecular parameters. The IUPAC-A polymer melt is the largely polydisperse, $\bar{M}_w/\bar{M}_n = 24.9$ and highly branched chain.¹⁹

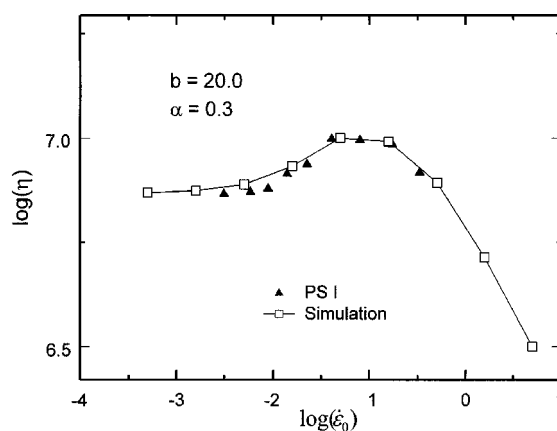


Figure 13. Comparison of the original FENE dumbbell model for the steady state elongational viscosity with the data of Münstedt¹⁸ for the polystyrene melt. The data of original FENE dumbbell are drawn for $\lambda_H = 19.9$ s and $nkT\lambda_H = 2,818,382$ Pa s. (Filled symbols represent the data of Münstedt¹⁸ and line-open symbols represents the simulation data)

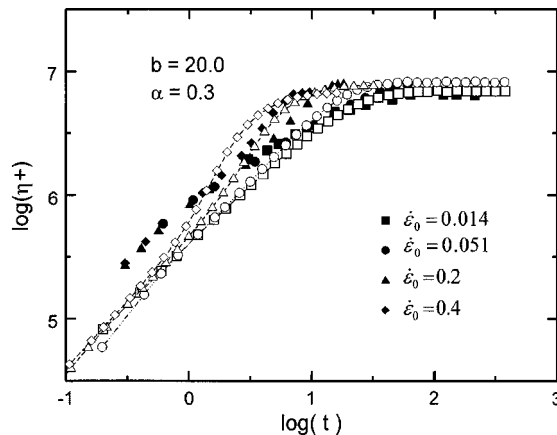


Figure 14. Comparison of the FENE dumbbell model for the growth of elongational viscosity with the data of Münstedt.¹⁸ The data of FENE dumbbell are drawn for the same parameters in Figure 13. (Filled symbols represent the data of Münstedt¹⁸ and line-open symbols represent the simulation data)

Whereas the polystyrene melt possesses a narrow molecular weight distribution, $\bar{M}_w/\bar{M}_n = 1.2$.¹⁸

From our study for the anisotropic FENE dumbbell models, we find that these models well describe the experimental results in steady state viscosity for shear flow and elongational flow. However, the FENE dumbbell models cannot reproduce the growth of viscosity of polymer solution and the melt in both flow fields. Besides the molecular parameters such as molecular weight, molecular weight distribution, and branching, there are several causes for the discrepancy in growth of viscosity between dumbbell models and experiments. 1) We oversimplify the polymer chain as dumbbell model that cannot take up an enormous number of configurations of polymer chain. 2) The diffusion equation for dumbbell model cannot represent the chain entanglement phenomena, by which the viscoelasticity of concentrated polymer solution and the melt is rigorously affected. 3) The averaged mobility tensor cannot correctly represent the anisotropy of polymer chain. In concentrated polymer solution and the melt, we can reasonably assume that the chain motion is governed not by averaged means but by the instantaneous configuration of individual chain.

Conclusions

We have investigated the viscosity of concentrated polymer solution and the melt using the Brownian dynamics simulation for anisotropic original FENE dumbbell model. The original FENE dumbbell model as well as FENE-P model described well the steady state viscosity of polymer solution and the melt in shear and elongational flow. Considering the simplicity of the dumbbell model in our study, we can probably predict the growth of viscosity in both flow fields by using a more realistic polymer chain model such as bead-spring chain model or bead-rod chain model. Furthermore, we can also obtain better simulation results by taking account of entanglement effect and introducing instantaneous mobility tensors.

Acknowledgment. Financial support (in part) from the Brain Korea 21 program is gratefully acknowledged.

References

1. de Gennes, P. J. *J. Chem. Phys.* **1979**, *55*, 572.
2. (a) Doi, M.; Edwards, S. F. *J. Chem. Soc. Faraday Trans. 2* **1978**, *74*, 1789. (b) Doi, M.; Edwards, S. F. *ibid.* **1978**, *74*, 1802. (c) Doi, M.; Edwards, S. F. *ibid.* **1978**, *74*, 1818. (d) Doi, M.; Edwards, S. F. *ibid.* **1979**, *75*, 38.
3. Doi, M.; Edwards, S. F. *The Theory of Polymer Dynamics*; Clarendon Press: Oxford, U. K., 1986; Ch. 6-7.
4. (a) Curtiss, C. F.; Bird, R. B. *J. Chem. Phys.* **1982**, *74*, 2016. (b) Bird, R. B.; Saab, H. H.; Curtiss, C. F. *ibid.* **1982**, *86*, 1102. (c) Saab, H. H.; Bird, R. B.; Curtiss, C. F. *ibid.* **1982**, *77*, 4758. (d) Bird, R. B.; Curtiss, C. F.; Armstrong, R. C.; Hassager, O. *Dynamics of Polymeric Liquids, Vol. 1: Fluid Mechanics, Vol. 2: Kinetic Theory*, 2nd ed.; John Wiley & Sons; Inc.: New York, U.S.A., 1987.
5. (a) Giesekus, H. *Rheol. Acta* **1982**, *21*, 366. (b) Giesekus, H. *J. Non-Newtonian Fluid Mech.* **1982**, *11*, 69. (c) Giesekus, H. *J. Non-Newtonian Fluid Mech.* **1983**, *12*, 367. (d) Giesekus, H. *J. Non-Newtonian Fluid Mech.* **1985**, *17*, 349.
6. Bird, R. B.; Wiest, J. M. *J. Rheol.* **1985**, *29*, 519.
7. Warner, H. R. Jr., Ph.D. Thesis, University of Wisconsin, Madison, 1971.
8. Bird, R. B.; Wiest, J. M. *Annu. Rev. Fluid Mech.* **1995**, *27*, 169.
9. Herrchen, M.; Öttinger, H. C. *J. Non-Newtonian Fluid Mech.* **1997**, *68*, 17.
10. Wiest, J. M. *Rheol. Acta* **1989**, *28*, 4.
11. Peterin, A. *Makromol. Chem.* **1961**, *44*, 338.
12. Ermak, D. L.; McCammon, J. A. *J. Chem. Phys.* **1978**, *69*, 1352.
13. Öttinger, H. C. *Stochastic Processes in Polymeric Fluids*; Springer: Berlin, Germany, 1996.
14. Kloeden, P. E.; Platen, E.; Shurz, H. *Numerical Solution of SDE Through Computer Experimentals*; Springer: Berlin, Germany, 1994; Ch. 5.
15. Öttinger, H. C. *Macromolecules* **1994**, *27*, 3415.
16. Tanner, R. I. *Trans. Soc. Rheol.* **1975**, *19*, 37.
17. Menezes, E. V.; Graessley, W. W. *Rheol. Acta* **1980**, *19*, 38.
18. Münstedt, H. *J. Rheol.* **1980**, *24*, 847.
19. Laun, H. M.; Münstedt, H. M. *Rheol. Acta* **1979**, *18*, 492.